Radiation Profiles in Extended Water Clouds. III: Observations

G. L. STEPHENS, G. W. PALTRIDGE AND C. M. R. PLATT

CSIRO Division of Atmospheric Physics, Aspendale, Victoria, Australia

(Manuscript received 3 October 1977, in final form 6 July 1978)

ABSTRACT

Six case studies of "uniform" planetary boundary layer clouds are reported where the solar and infrared radiation fields, liquid water content, drop-size distributions and temperature and humidity profiles were measured simultaneously. The measurements are compared with theoretical prediction from a detailed radiative transfer model in an attempt to verify the performance of the model and its associated parameterization schemes (Parts 1 and 2). The measurements support the parameterization of both shortwave and longwave radiative characteristics in terms of vertical liquid water path (LWP) i.e., without the need to define cloud drop-size distributions. Within experimental error, there are no significant discrepancies between theory and measurement. However, there is some evidence in the present study, supported by measurements of others in (generally) thicker and denser clouds that solar absorption is in excess of theoretical prediction.

1. Introduction

This paper examines the albedo, shortwave absorption, vertical distribution of shortwave and longwave fluxes and the 8–13 μm downward radiance profiles measured in a number of planetary boundary layer clouds observed over the past six years by the CSIRO Division of Atmospheric Physics. They were selected for analysis because of their uniformity and availability of fairly complete microphysical data which would allow comparison with theory.

The data were obtained during three series of flights on the CSIRO Division of Cloud Physics' DC-3 aircraft off the Australian east coast at Coff's Harbour (30°S) in December 1971, Merimbula (37°S) in February 1973 and Hobart (43°S) in May 1976. The flight patterns and aircraft instrumentation were similar to those described by Paltridge (1974a). The instruments included upward and downward viewing glass-covered (shortwave) and polythene-covered (shortwave plus longwave) pyradiometers, as well as a narrow-beam radiometer measuring the nadir radiance in the 10–12 μm or 8–13 μm regions (Platt, 1976).

Drop-size distributions were measured by the slide-impactor techniques described by Clague (1965). During the last series at Hobart, a Knollenberg spectrometer (Knollenberg, 1970) was also available to measure the drop-size distributions at the rate of 1 s^{-1}. Liquid water content (LWC) information was obtained by integration of the drop-size distributions. The data obtained during the Hobart series were recorded and stored on disc and magnetic tape via an onboard Hewlett–Packard 2100A computer. This provided simultaneous 1 min/averages of the four radiation flux values, cloud albedo, 8–13 μm (or 10–12 μm) nadir radiances as well as LWC, pressure, wet-bulb and dry-bulb temperatures and mixing ratio. The two earlier series of flights relied on chart recordings of the data to provide averages.

The eight cloud layers discussed here satisfied the following specific requirements: 1) they had well-defined tops and bases; 2) no other cloud existed above or below the deck of interest; 3) they were extensive enough to allow the aircraft to fly horizontally over or through them for several minutes; and 4) they were stable enough to obtain complete radiation profiles. Only clouds over the sea were sampled to ensure a constant upwelling radiant flux below the cloud base. In fact, during all the series, measurements were attempted only when a cloud layer appeared to possess the definable characteristics described above. The number of such occasions was small and "after the event" analysis reduced the number of usable case studies to eight. Of these, only six (those of Merimbula and Hobart) had reasonably complete microphysical data.

The physical characteristics of the clouds varied from one series of flights to another. In particular, the clouds sampled at Coff's Harbour and, to a lesser extent, at Merimbula during the summer season possessed obviously turreted tops. The cloud layers of the third series at Hobart (during winter) were much flatter. They were wetter than those of the first two series and were much more stable in that they persisted for several hours. This stability, coupled with the availability of the Knollenberg instrument, ensured that the Hobart data are the most reliable and complete.

2. Case study summary

Table 1 gives the broad meteorological characteristics of the eight cloud layers including the inversion strength, the mixing ratio difference across the inversion

0022-4928/78/2133-2141$05.00

TABLE 1. Gross character of planetary boundary layer clouds investigated.

Flight no.	Date	Thickness (km)	Base height (km)	Temperature (°C)			Mixing ratio (g kg^{-1})			T_s (°C)
				T_t	T_b	ΔT	W_t	W_b	ΔW	
1	2 Dec 1971*	0.65	1.03	7.5	11	4.5	8	9	6.0	23
2	5 Dec 1971*	0.84	0.61	12	17	5.5	10.2	13	4.5	23
5	8 Feb 1973	0.32	1.51	4	5	6	7	7.2	6.5	21
9	12 Feb 1973	0.23	1.90	−1	1	6	5	6	3.5	21
10	12 Feb 1973	0.18	2.17	0	1	5.6	5.6	5.5	3.5	21
7	10 May 1976	0.4	1.07	−1.4	1.8	2.2	3.7	4.0	0.9	8
8	12 May 1976	0.48	1.13	−2.6	−0.4	5.5	3.5	3.7	2.9	7.6
9	13 May 1976	0.55	0.98	−2.1	1.3	7.9	3.5	3.7	3.4	7.6

T_t, T_b, W_t, W_b are the temperature and mixing ratios at the top and base of the cloud layer, respectively.
ΔT is the inversion strength (T_0-T_t); and ΔW is the mixing ratio difference across the inversion (W_t-W_0).
* From Paltridge (1974).

and the sea surface temperature. The definition of the variables listed can be obtained from Fig. 1. The sea surface temperature T_s was obtained by extrapolating adiabatically down from the cloud base, through the lowest measured temperature (~150 m from the sea surface) to the surface. Table 2 lists the broad shortwave radiative characteristics determined from measurements at cloud top and base. The solar zenith angles quoted in the table were the means appropriate to the time during which the profile was obtained. The cloud albedo varied from 0.495 to 0.746 and generally increased with increasing zenith angle. However, this variation depends on cloud thickness and density. The cloud absorptions varied from 0 to 0.2 with an average of 0.087 for the eight studies tabulated. The incident shortwave flux at the cloud top also appears in the Table.

Table 3 lists the drop-size distributions which were available for six of the case studies. Those from the slide impactor are an average of a number of slides taken in a batch during a 1–2 min period at a given level. The Knollenberg distributions obtained at Hobart are 4 min averages, some of which overlap with "simultaneous" batches of impactor distributions. Fig. 2 is a plot of the mode radius of the distributions in Table 3 as a function of LWC. Also included (solid triangles) are those measured in similar clouds which were not suitable for further analysis. The solid points are those of Paltridge (1974a) for data obtained at Coff's Harbour and Merimbula. The solid squares are the impactor distributions which overlap with the Knollenberg distributions obtained at Hobart (the crosses) and are joined to the relevant Knollenberg distributions by a solid line.

Three points can be made about Fig. 2. First, the mode radius of the distribution generally increases with increasing LWC. Second, the Knollenberg versus impactor comparisons are reasonable in view of the entirely different character of the measurements (the impactor is essentially a point measurement not of exactly the same volume of cloud). Third, the Hobart clouds were generally wetter and had flatter drop-size distributions than those measured previously.

Finally, Fig. 3 is an example of the actual radiative flux profiles measured in one of the Hobart clouds. The absolute accuracy is about ±10 W m^{-2} for a single pyradiometer measurement. The measurements involving differences of pyradiometer outputs are better represented by rms errors. Thus assuming entirely random errors, the rms errors of longwave flux, shortwave and longwave absorptions are ±14, ±20 and ±28 W m^{-2}, respectively. These errors are likely to be upper limits for the probable error since some of the absolute error is systematic. These systematic errors may (or may not) cancel for measurements involving flux differences, making the expected error even less than the quoted figures above. Averaging the radiometer outputs over time intervals exceeding the time constant of the pyradiometers (~15–20 s) will further reduce these error estimates. For the Merimbula and

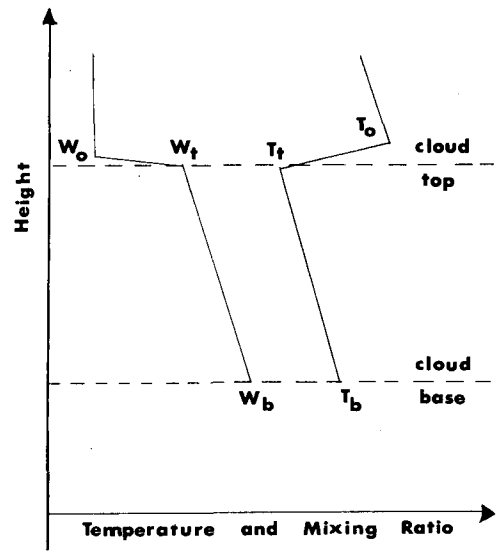

FIG. 1. The gross character of the clouds investigated.

TABLE 2. Measured shortwave radiation parameters of several cloud layers investigated.

Location	Date of flight	Flight no.	Mean solar incidence μ_0	$F_S^{\downarrow}$ at cloud top (W m^{-2})	Albedo	Transmission	Absorption
Coff's Harbour	2 Dec 1971*			1130	0.496	0.575	0.000
(31°S)	5 Dec 1971			980	0.586	0.404	0.061
Merimbula	8 Feb 1973	5	0.81	880	0.674	0.506	0.045
(37°S)	12 Feb 1973	9	0.86	930	0.495	0.538	0.043
	12 Feb 1973	10	0.78	1020	0.488	0.671	0.061
Hobart	10 May 1976	7	0.25	220	0.677	0.122	0.200
(42°S)	12 May 1976	8	0.31	300	0.746	0.119	0.135
	13 May 1976	9	0.47	410	0.554	0.308	0.138

* Paltridge (1974).

Coff's Harbour case studies, the quoted error limits are reduced by a factor of 2. The Hobart case studies were averaged over longer periods and the respective error limits are reduced by a factor of 3.

3. Comparison between theory and observation

a. Shortwave absorption and cloud albedo

It was shown in Part 2 (see Fig. 3 of that paper) that shortwave absorption is primarily an increasing function of the vertical liquid water path (LWP) in the cloud with relatively little variability arising from cloud type or position. Further it was shown that the fractional absorption is not highly variable with solar position except for large zenith angles ($\theta_0 > 60°$).

Thus the solid line of Fig. 4 is the theoretical fractional absorption as a function of LWP determined for zero solar zenith angle. The shading about that line is the expected variability which might arise from differences in cloud type. The various points on the diagram are the experimental values obtained from the present study, each of which could be subject to substantial error. Data from other sources are also included. The vertical lines are the error bars about the measurements in similar planetary boundary layer clouds by Neiburger (1949); the shaded squares and horizontal lines are values from Drummond and Hickey (1971) and Reynolds *et al.* (1975), where the liquid water paths have been intuitively estimated from cloud types.

The differences between the theoretical and experimental determinations of shortwave absorption often fall outside these error limits. In particular, the measurements by Reynolds *et al.* and Drummond and Hickey in generally thicker and denser clouds suggest that absorption may be "anomalously" high. In this context, it may be significant that the absorption of the three Hobart clouds (the densest of the present study) were all higher than the theoretical estimates—especially in view of the low solar elevation during these measurements which would tend to lower the theoretical absorption. If such anomalous absorption does exist, it could be explained by the presence of substances other than liquid water or water vapor in the cloud. Clouds are not necessarily pure liquid water or ice (Twomey, 1976).

Table 4 lists the measured albedo and the fractional absorption and transmission for the six case studies. The calculated values determined by the detailed theoretical model described in Part 1 are included in parentheses. The differences in the absorption comparisons indicated in the table were described above. The disagreement in one case (10 May) is much larger than the other cases and may be due to the lower solar elevation (and hence smaller signal) during those measurements. Comparison between the theoretical and measured cloud albedo for the six case studies are generally within the limits imposed by experimental uncertainty.

b. Profiles of shortwave heating and total IR cooling

Fig. 5 shows a comparison of measured and computed profiles of shortwave and longwave heating for one of the Hobart clouds.

The solid curve on the diagram is the heating or cooling profile calculated by the detailed theoretical model (Part 1). These calculations were performed using the average drop-size distributions recorded at each level, the observed surface albedo, and the mean solar zenith angle estimated from the recorded time averaged between the horizontal traverses at the cloud top and base. The temperature and moisture profiles measured in and about the cloud by the aircraft, supplemented by the radiosonde data for Hobart (0900 LT) were used to calculate the clear-air fluxes at the cloud boundaries (see Part 1). These theoretical clear-air fluxes were generally determined within ± 14 W m^{-2} of the measured values at the cloud top.

The rms error bars on the measured data points are large and are indicative of the difficulties involved with such measurements. Nevertheless, the correspondence with theory is surprisingly good, especially in terms of the concentration of heating and cooling toward the cloud top. The discrepancy in the magnitude of the

TABLE 3. The measured average drop-size distribution in six planetary boundary layer clouds.

Height (ft)	Liquid water content* (g m^{-3})	Droplet diameter (μm) 4.5	7.5	10.5	13.5	16.5	19.5	22.5	25.5	28.5	31.5	34.5	37.5	40.5	43.5	46.5	49.5
10 May 1976																	
1460	0.065	—	—	—	0.01	0.05	0.77	1.94	2.16	1.55	0.54	2.12	0.03	—	—	—	—
1370	0.267	0.01	—	0.21	0.14	6.13	18.58	16.42	7.23	1.75	0.37	0.07	0.02	0.01	—	—	—
1280	0.267	0.02	0.01	0.52	0.31	13.14	25.63	14.67	4.20	0.73	0.16	0.03	0.01	—	—	—	—
1190	0.181	0.02	0.02	0.83	0.98	16.31	18.68	7.69	1.84	0.34	0.07	0.02	0.01	0.01	—	—	—
1100	0.133	0.03	0.03	0.62	3.07	18.74	13.34	3.80	0.82	0.17	0.04	0.02	0.01	—	—	—	—
12 May 1976																	
1460	0.544	0.03	0.02	0.06	0.18	15.24	48.03	34.17	9.15	1.85	0.50	0.12	0.06	0.03	0.02	0.01	0.01
1400	0.266	0.03	0.02	0.10	0.29	14.77	30.49	7.26	1.60	0.41	0.14	0.08	0.04	0.03	0.02	0.03	0.02
1310	0.171	0.09	—	0.02	0.23	7.47	8.40	1.97	0.90	0.60	0.52	0.45	0.44	0.21	0.36	0.34	0.29
1220	0.183	0.12	0.01	0.31	0.72	7.81	4.44	1.23	0.86	0.75	0.60	0.59	0.51	0.47	0.41	0.38	0.30
1130	0.055	0.02	0.01	0.31	1.58	10.49	4.80	0.78	0.14	0.07	0.07	0.62	0.01	0.02	0.01	—	—
13 May 1976																	
1460	0.617	0.03	0.02	0.06	0.15	6.93	38.53	40.15	16.80	3.08	0.93	0.24	0.09	0.04	0.02	0.02	0.01
1400	0.200	0.01	0.01	0.04	0.18	13.53	27.07	7.95	1.49	3.67	0.11	0.04	0.02	0.03	0.01	0.01	—
1310	0.035	0.01	—	0.31	0.26	4.13	4.04	0.83	0.24	0.08	0.03	0.02	0.01	0.01	0.01	0.01	0.01
1220	0.074	0.02	0.01	0.83	0.52	8.20	8.20	1.88	0.49	0.16	0.07	0.03	0.02	0.02	0.02	0.01	0.01
1130	0.139	0.03	0.02	0.47	1.27	16.55	17.58	3.19	0.82	0.22	0.10	0.04	0.03	0.03	0.02	0.02	0.01
1040	0.096	0.03	0.02	0.62	2.04	15.79	8.53	1.76	0.52	0.17	0.10	0.06	0.03	0.03	0.03	0.03	0.01

* The distributions represent the 4 min average along the horizontal traverse specified by the height (samples were recorded at a rate of 1 s^{-1}). The units of the distribution are number of drops cm^{-3} (3 μm)$^{-1}$ radius interval.

TABLE 3—(*Continued*)

Flight 5: 8 February 1973

Height (km)	Number of slides**	Liquid water content (g m^{-3})	Droplet diameter (μm) 4.0	6.7	8.8	11.0	13.0	15.1	17.3	19.5	21.8	24.2	26.6	29.0
1.78	6	0.244	—	0.73	2.33	4.13	8.68	13.33	18.68	5.80	2.13	2.57	1.65	0.85
1.68	9	0.207	—	0.63	1.93	4.12	6.83	7.94	9.34	4.10	1.87	2.79	2.17	1.03
1.60	9	0.140	—	0.22	1.38	8.68	28.34	26.70	10.39	1.91	0.41	0.24	0.13	0.16
1.54	2	0.123	—	0.65	5.05	8.50	9.15	9.60	6.90	3.70	2.05	2.60	0.70	0.60
1.51	8	0.102	0.23	3.31	13.34	18.43	9.94	6.16	6.21	5.78	5.08	0.97	0.44	0.40

Flight 9: 12 February 1973

Height (km)	Number of slides	Liquid water content (g m^{-3})	Droplet diameter (μm) 3.9	6.6	8.8	10.9	13.0	15.1	17.2	19.4	21.8	24.1	26 5	28.8
2.11	9	0.23	—	0.27	0.73	1.22	3.46	7.79	46.28	17.92	2.34	0.54	0.06	0.06
2.08	7	0.157	—	0.09	1.09	0.84	19.59	35.41	21.63	3.79	0.56	0.13	0.01	0.01
2.02	8	0.146	—	0.04	1.45	2.13	2.57	26.84	17.05	2.94	0.26	0.05	0.04	0.03
1.96	4	0.043	0.08	7.8	25.75	16.9	12.2	0.33	0.45	0.28	0.05	0.03	0.08	—

Flight 10: 12 February 1973

Height (km)	Number of slides	Liquid water content (g m^{-3})	Droplet diameter (μm) 4.4	7.4	9.9	12.4	14.8	17.3	19.9	22.7	25.5	28.3	31.0	33.8
2.32	8	0.242	1.23	1.69	1.59	1.70	2.14	2.79	6.73	6.94	3.68	2.98	1.36	0.95
2.26	5	0.212	2.76	1.96	1.68	1.96	3.96	4.54	8.06	7.22	3.58	2.46	0.78	0.34
2.19	8	0.025	3.45	11.06	14.90	4.91	0.58	0.25	0.25	0.15	0.08	0.10	0.03	0.01

** The distributions are averaged over the given number of slide samples. The units of the distribution are number of drops cm^{-3} (2.5 μm) radius interval.

TABLE 3—(*Continued*)

Flight 5: 8 February 1973

Droplet diameter (μm) 31.3	33.7	36.0	38.4	40.8	43.1	45.3	47.1	49.3	52.3	54.6	58.3	61.4
0.62	0.38	0.38	0.15	0.08	0.12	0.10	0.05	—	—	—	0.02	0.02
0.70	0.46	0.46	0.21	0.19	0.07	0.03	0.02	0.02	0.03	0.03	0.01	—
0.09	0.11	0.07	0.04	0.01	0.02	—	0.01	0.01	—	—	—	—
0.25	0.10	0.05	0.05	—	—	—	0.05	—	—	—	0.03	0.01
0.21	0.14	0.08	0.08	0.08	0.01	0.01	—	0.02	0.03	0.03	0.03	0.01

Flfght 9: 12 February 1973

Droplet diameter (μm) 31.2	35.9	40.5	42.9
0.04	—	0.01	—
0.03	—	—	—
—	0.01	—	0.01
—	—	0.03	0.03

Flight 10: 12 February 1973

Droplet diameter (μm) 36.5	39.3	42.2	44.7	47.4	50.1	52.7	55.4	58.5	68.5
0.51	0.19	0.28	0.05	0.05	0.05	0.01	0.06	0.03	0.01
0.20	0.30	0.16	0.02	0.08	0.02	—	—	—	—
0.01	0.01	—	—	—	—	—	—	—	—

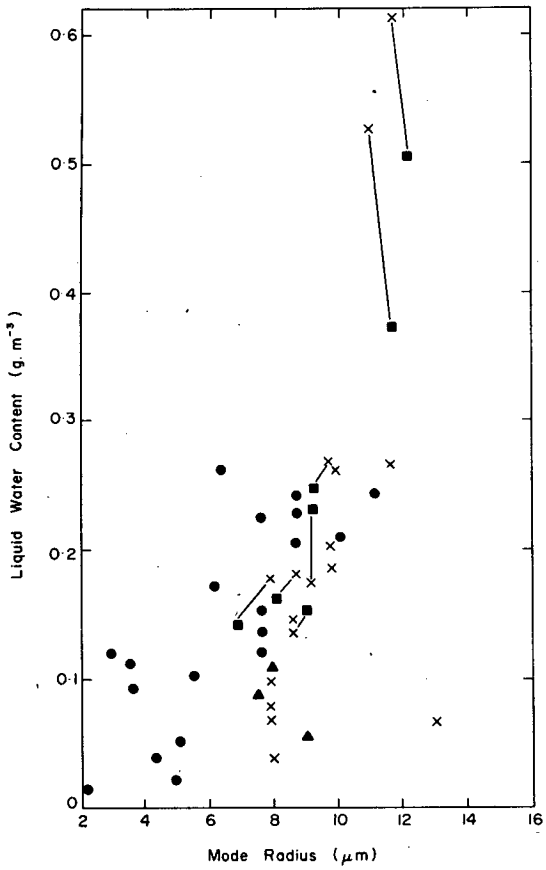

FIG. 2. The liquid water content of a cloud as a function of mode radius of the distribution. The crosses are the 4 min average Knollenberg values. All other points are an average of a number of slides taken in a batch. The impactor distributions measured simultaneously with Knollenberg distributions are connected by solid lines.

theoretical and measured shortwave heating is due to the presence of anomalous absorption. The most significant point is that the maximum shortwave heating is of the same order as the IR cooling, and is effective over much the same depth into the cloud. This feature is more evident in Table 5 in which the theoretical and measured total longwave and shortwave flux divergences are compared for the three Hobart clouds. The measured shortwave divergences are anomalously large compared to the theoretical estimates and are, in fact, *larger* than the measured longwave divergences, although the latter measurements are subject to larger experimental error. The theoretical longwave divergences are much larger than the measured values and is due, in part, to the fact that the calculated clear-air downward fluxes at the cloud top were systematically smaller by approximately 10 W m^{-2} of the measured values. This systematic difference may be due to the failure of the measurements to accurately determine the structure of the moisture discontinuity and temperature inversion at the cloud top. However, these differences are more likely to result from systematic errors in the pyradiometer outputs which have not cancelled. While the same may be true for the shortwave flux divergences, the extent of any likely systematic error will be smaller and cannot explain the observed discrepancies between the theoretical and measured shortwave absorption estimates. It is possible that the present measuring techniques will not provide the longwave flux divergences within $\pm$10–20 W m^{-2}. Nevertheless, it is clear from the comparisons of Table 5 that shortwave heating is an important parameter which must be taken into account when studying the radiative effects on the dynamics of stratiform clouds. During daytime, it will tend to lessen the radiatively induced instability of the cloud and presumably the erosion and entrainment through the inversion (Paltridge, 1974b; Lilly, 1968; Deardorff, 1976).

c. *IR window radiances*

Of the eight case studies reported here, only two from the Hobart series have nadir radiance measurements covering the complete window region from 8–13 μm, and they are presented in Figs. 6a and 6b. The radiance data for the other six were limited to the 10–12 μm region and have been discussed elsewhere (Platt, 1976; Stephens, 1976).

The theoretically calculated radiance profiles appear as solid lines on each diagram. The calculations were performed using eight spectral intervals from 6.9 to 16.7 μm since the filter transmission characteristics, primarily centered between 8 and 13 μm, extended out to these wavelengths. The clear-air radiances at the cloud boundary were calculated by the method described in Part 1. These theoretical radiances impinging

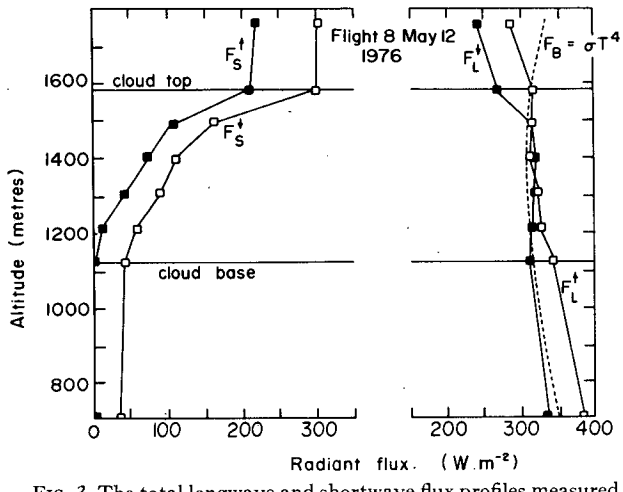

FIG. 3. The total longwave and shortwave flux profiles measured in three Sc cloud layers. $F_S^{\uparrow,\downarrow}$, $F_L^{\uparrow,\downarrow}$ and F_B are, respectively, the shortwave and longwave fluxes and blackbody flux. Each point is a 4 min average value.

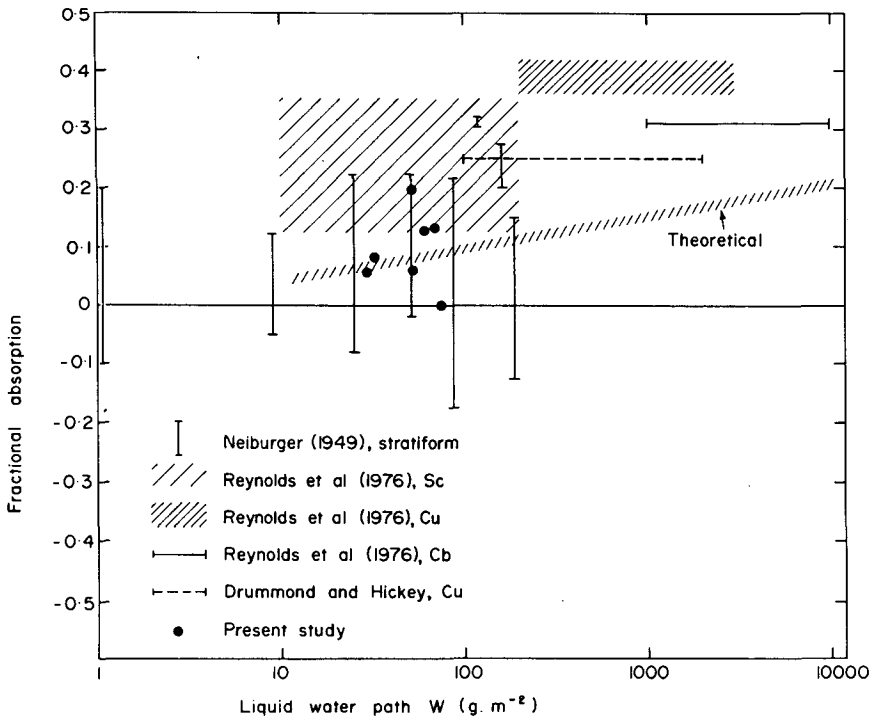

FIG. 4. Comparison between measured and calculated fractional shortwave absorption as a function of liquid water path. The shading about the line is the expected variability which may arise from differences in cloud type. The horizontal and vertical lines, boxes and points are measured values.

the cloud top were normalized to the measured values. In both cases this adjustment was small. This ensured a correct starting point for the verification.

The experimental points are the averages of each 4 min run at a given level in the cloud. The comparisons show good agreement between the theoretical and measured radiance profiles. In particular, the calculated profile adequately describes the level at which the cloud may be considered to be radiating as a blackbody. In Fig. 6a, the LWC is small at the cloud top and the radiance values are almost black at a depth of 200 m. The cloud described in Fig. 6b, by contrast, is extremely moist in its upper layers and assumes blackbody values at a depth of 100 m.

TABLE 4. The measured and calculated (in parentheses) cloud albedo, transmission and absorption in six planetary boundary layer clouds.

Date of flight	Albedo	Transmission	Absorption
5 Feb 1973	0.674 (0.668)	0.506 (0.495)	0.045 (0.110)
12 Feb 1973	0.495 (0.440)	0.538 (0.591)	0.043 (0.078)
12 Feb 1973	0.488 (0.439)	0.671 (0.692)	0.070 (0.076)
10 May 1976	0.677 (0.654)	0.122 (0.316)	0.200 (0.030)
12 May 1976	0.746 (0.757)	0.119 (0.186)	0.135 (0.057)
13 May 1976	0.654 (0.678)	0.208 (0.239)	0.138 (0.083)

d. The total IR flux emissivity and the 10–12 μm radiance emissivity

In Fig. 7 the measured "effective total downward emissivities" for the three Hobart case studies are shown as a function of liquid water path. The open circles are the measured emissivities published previously by Paltridge (1974a). The emissivities were determined using the mean temperature averaged along the path from the cloud top to the level of measurement. The liquid water paths were similarly determined by integration of the LWC along the same path. The more recent data from Hobart apply to the 4 min average flux measurements whereas those of the first two series were 1 min averages from chart recordings.

The solid curve in Fig. 7 is the parameterized relation determined from a number of theoretical computations (see Part 2). The agreement between observation and theory is poor. The discrepancy can be attributed almost entirely to experimental error. The error in liquid water path may be as large as 10 g m^{-2} because of the presence of cloud turreting. Further, the emissivity definitions involve differences between large and almost equal measured flux values. The extent of the experimental error that should be attached to these points has been discussed previously by Paltridge (1974a). The errors are compounded by the need to take a ratio of two of these values.

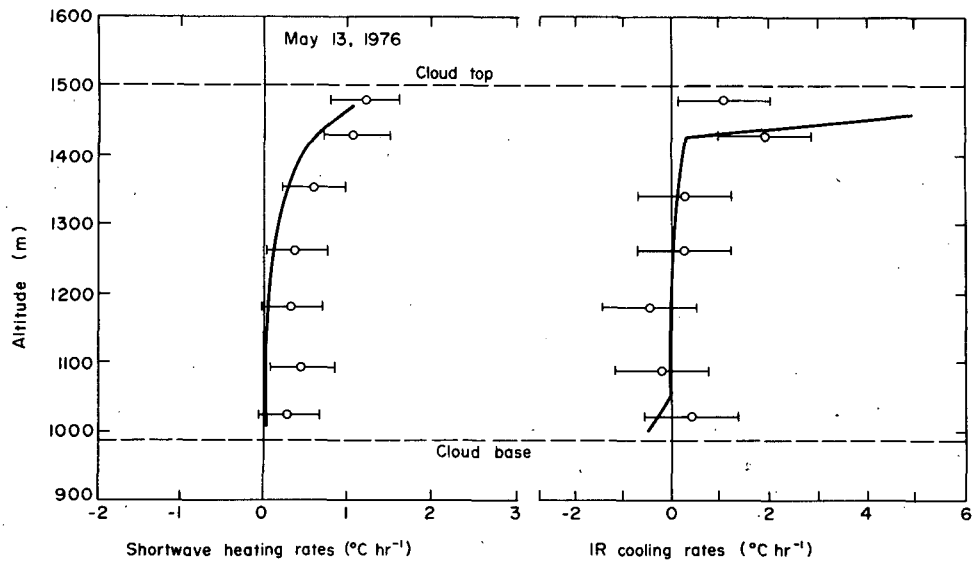

FIG. 5. The shortwave and longwave heating and cooling rate profiles measured in the cloud layer sampled on 13 May 1976. The extent of the rms experimental error is shown by the horizontal lines. The solid curve is the theoretically calculated profile.

Fig. 8 shows the measured emissivities determined from several nadir radiance profiles for the 10–12 μm region. Details of the comparison of these measured profiles with theoretical calculations were described by Stephens (1976). The solid line is the parameterized profile for the entire atmospheric window region as described in Part 2. The mass absorption coefficient for the window region was determined in Part 2 as $a_0^{\downarrow}=0.116$ for diffuse radiation. This coefficient is smaller by a factor of 1.66 for vertical radiation (Elsasser, 1942).

The agreement between the 10–12 μm and parameterized estimates of total window emissivity is good. This implies that the 10–12 μm measurements are indeed representative of the total window emissivity, which in turn (as shown in Part 2) is the prime determinant of the total emissivity of the cloud. The emissivities determined using the nadir radiance values do not suffer from the large uncertainties associated with the total flux measurements and are therefore more reliable.

TABLE 5. A comparison between the measured and calculated longwave and shortwave flux divergences for the three Hobart cloud layers.

Date of flight	Measured (W m^{-2}) shortwave (±7)*	longwave (±10)*	Calculated (W m^{-2}) shortwave	longwave
10 May 1976	44	−10	9	−55
12 May 1976	38	−40	20	−55
13 May 1976	57	−52	35	−72

* rms experimental error (W m^{-2}) for 4 min averages.

4. Conclusions

There is some evidence in the case studies presented here, supported by others in (generally) thicker and denser clouds, that solar absorption is in excess of

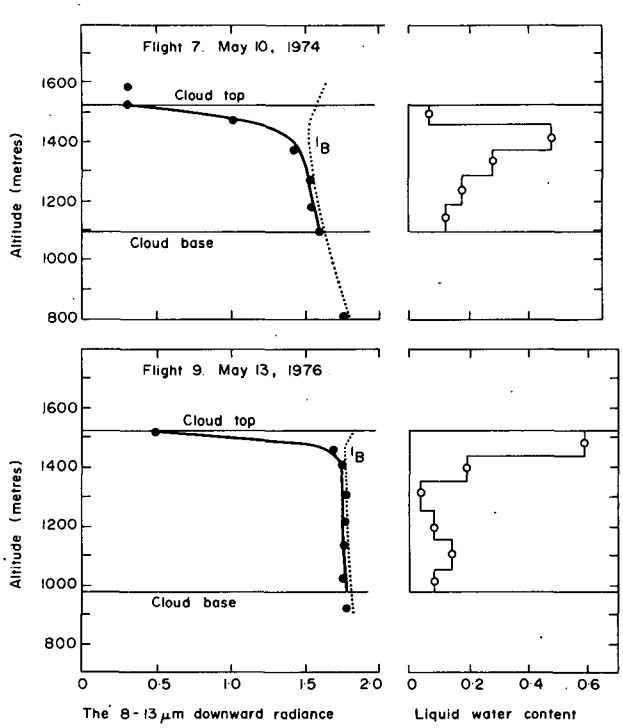

FIG. 6. The measured 8–13 μm nadir radiance profiles and LWC as a function of altitude. Included on the diagram are the theoretically calculated radiance profiles (solid lines) and the blackbody curve (dotted lines).

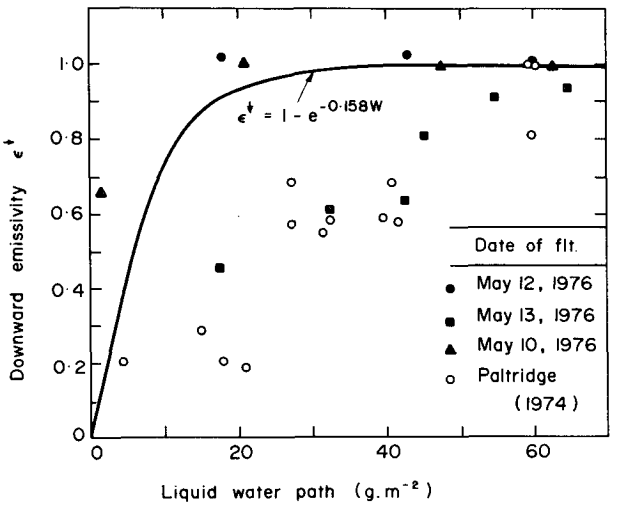

FIG. 7. Experimental values of total emissivity as a function of liquid water content. The solid line is the emissivity–liquid water path relation derived in Part 2.

theoretical prediction (anomalous absorption). The parameterization of shortwave absorption must rely on theoretical estimates until this anomaly is more thoroughly investigated.

Large experimental errors are present in the shortwave and longwave heating and cooling rate profiles. Despite this, both theory and observation show a pronounced shortwave heating and longwave cooling in the upper layers of the cloud. Comparison of the measured shortwave and longwave flux divergences indicate that the solar heating in a cloud may be equally important as the longwave cooling. This is not as evident from the theoretical values which indicate that the IR cooling is more dominant. Comparison between the theoretical and measured cloud albedo for the six case studies are good and within experimental uncertainty.

The theoretically deduced total flux emissivities generally do not agree with the measured estimates. Experimental inaccuracies could easily account for this discrepancy. The emissivities measured by the accurate narrow-beam radiometer in the 10–12 μm region match the theoretical (parameterized) estimates closely. This provides a useful verification of the emissivity parameterization with accurate and reliable measurements.

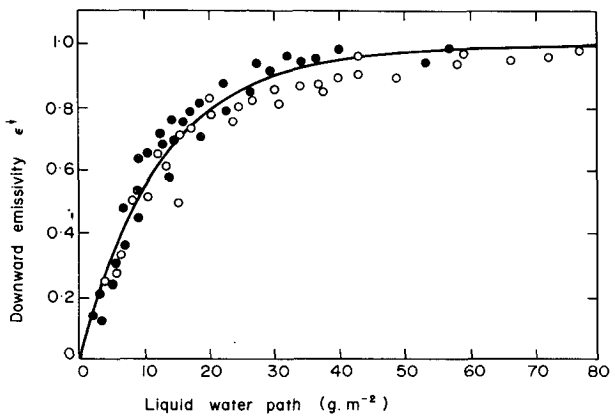

FIG. 8. Experimental values of 10–12 μm emissivity determined from nadir radiance measurements as a function of liquid water path. The solid line is the parameterized total window emissivity derived in Part 2. The solid points are the measured values obtained from four of the six case studies. The open circles were obtained from similar cloud layers (Platt, 1976).

REFERENCES

Clague, L. F., 1965: An improved device for obtaining cloud droplet samples. *J. Appl. Meteor.*, **4**, 549–551.

Deardorff, J. W., 1976: On the entrainment rate of stratocumulus-topped mixed layers. *Quart. J. Roy. Meteor. Soc.*, **102**, 563–582.

Drummond, A. J., and J. R. Hickey, 1971: Large-scale reflection and absorption of solar radiation by clouds as influencing earth radiation budgets. New aircraft measurements. *Preprints Int. Conf. Weather Modification*, Canberra, Amer. Meteor. Soc., 267–276.

Elsasser, W. M., 1942: Heat transfer by infrared radiation in the atmosphere. *Harvard Meteor. Stud.*, No. 6, Harvard University Press, 107 pp.

Knollenberg, R. G., 1970: The optical array: An alternative to scattering or extinction for airborne particle size determination. *J. Appl. Meteor.*, **9**, 86–103.

Lilly, D. K., 1968: Models of cloud topped mixed layers under a strong inversion. *Quart. J. Roy. Meteor. Soc.*, **94**, 292–309.

Neilburger, M., 1949: Reflection, absorption and transmission of insulation by stratus clouds. *J. Meteor.*, **6**, 98–104.

Paltridge, G. W., 1974a: Infrared emissivity, short wave albedo and the microphysics of stratiform water clouds. *J. Geophys. Res.*, **79**, 4053–4058.

——, 1974b: Atmospheric radiation and the gross character of stratiform cloud. *J. Atmos. Sci.*, **31**, 244–250.

Platt, C. M. R., 1976: Infrared absorption and liquid water content in stratocumulus clouds. *Quart. J. Roy. Meteor. Soc.*, **102**, 515–522.

Reynolds, D. W., T. H. von der Haar and S. K. Cox, 1975: The effect of solar radiation absorption in the tropical troposphere. *J. Appl. Meteor.*, **14**, 433.

Stephens, G. L., 1976: The transfer of radiation through vertically non-uniform stratocumulus water clouds. *Contrib. Atmos. Phys.*, **49**, 237–254.

Twomey, S., 1976: Computations of the absorption of solar radiation by clouds. *J. Atmos. Sci.*, **33**, 1087–1091.